

River delta eco-morphodynamics under changing scenarios. The case of Lake Turkana, Kenya

Simone Zen¹, Paolo Perona², and Encarni Medina-Lopez¹

¹The University of Edinburgh

²École polytechnique fédérale de Lausanne - EPFL

November 24, 2022

Abstract

In this work we explore the impact that changes in local climate and river hydrology have on the morphodynamics of a river delta, particularly focusing on the evolution of the delta generating at the lake inlet. We investigated the case of the delta in the lower reach of the Omo River in Ethiopia, which flows into Lake Turkana, Kenya. The lake is the fourth largest lake and the largest desert lake in the world. This case study is of particular interest because within the last decades three dams have been built within the Omo basin. To quantify changes in land use and river morphology and relate these to river hydrology we collect a historical dataset by combining information from different satellite sources. We observed that the amount of bare sediments progressively diminished and the biomass became more dense compared to the existence of sparse biomass in the past. We argue that this is due to the new river hydrology and sediment load imposed by the dam, which increased sediment erosion by deepening the channel. The dam also increased the low flow and reduced peak during flood season reducing the natural oscillations of the water table and the possibility to plant was removed during floods. We also indicate that the new hydrology and reduced sediments have changed, respectively, the downstream (e.g. lake level), and upstream (e.g. mouth bar deposition) boundary conditions controlling the evolution of the delta structure. As a result, the delta morphology became less dynamic and less complex.

1 **River delta eco-morphodynamics under changing**
2 **scenarios. The case of Lake Turkana, Kenya**

3 **Simone Zen¹, Paolo Perona^{1,2}, Encarni Medina-Lopez¹**

4 ¹School of Engineering, Institute for Infrastructure and Environment, The University of Edinburgh, UK

5 ²Ecole Polytechnique Fédérale de Lausanne, Switzerland

6 **Key Points:**

- 7 • This paper analyses the impact of local climate, river hydrology, and the construction
8 of three dams on river delta morphodynamics.
- 9
- 10 • Satellite imagery allowed us to quantify changes in land use and river morphology,
11 and relate these to climate change and river hydrology.
- 12
- 13 • The dams diminished the amount of bare sediments, increased the density of biomass
14 and low flow, and reduced the peak during flood season.

Corresponding author: E. Medina-Lopez, emedina@ed.ac.uk

Abstract

In this work we explore the impact that changes in local climate and river hydrology have on the morphodynamics of a river delta, particularly focusing on the evolution of the delta generating at the lake inlet. We investigated the case of the delta in the lower reach of the Omo River in Ethiopia, which flows into Lake Turkana, Kenya. The lake is the fourth largest lake and the largest desert lake in the world. This case study is of particular interest because within the last decades three dams have been built within the Omo basin. Among these, the Gibe III dam had a huge impact on the river hydrology and the sediment supply. To quantify changes in land use and river morphology and relate these to climate change and river hydrology we collect a historical dataset by combining information from different satellite sources. We observed that the amount of bare sediments progressively diminished and the biomass became more dense compared to the existence of sparse biomass in the past. We argue that this is due to the new river hydrology and sediment load imposed by the dam, which increased sediment erosion by deepening the channel. The dam also increased the low flow and reduced peak during flood season reducing the natural oscillations of the water table and the possibility to plant was removed during floods. We also indicate that the new hydrology and reduced sediments have changed, respectively, the downstream (e.g. lake level), and upstream (e.g. mouth bar deposition) boundary conditions controlling the evolution of the delta structure. As a result, the delta morphology became less dynamic and less complex.

Plain Language Summary

This paper studies the river Omo in Ethiopia and lake Turkana in Kenya. . The lake is the fourth largest lake and the largest desert lake in the world. We want to understand the impact that the construction of several dams on river Omo have had on the natural behaviour of lake Turkana. We used satellite imagery to study the area of interest over the past decades. The amount of sediment in the river delta reduced with the presence of dams. These also limited the natural oscillations in the water level of the lake. This meant that local farmers could not plant during flood season, as they used to, after the dams were built. The dams also changed the shape of the river mouth from its natural conditions.

1 Introduction

Fluctuations in lake levels and sediment load carried by the river that flows into the lake are the two main factors controlling lake delta dynamics (Haack, 1996). When a river reaches a basin, the backwater effect modifies the water flow from uniform to nonuniform inducing changes in the flux of channel bed material according to river flow conditions. During low-medium flows, the velocity decreases, suspended sediment is deposited, and the river channel tends to aggrade forming wider cross sections. On the other hand, when the river flow is high, the high velocity promotes channel bed erosion and channel avulsion, generating new fluvial distributary channels (Nittrouer et al., 2012). With time, sediment deposits forming mouth bars can be remobilized during subsequent high flow event thus promoting channel bifurcations (Edmonds & Slingerland, 2007). If the system is not disturbed by external forcing such as waves or tides, the channels of the bifurcation will experience avulsion and form new distributary channels, where a new mouth bar will be deposited originating a new bifurcation. Subsequently, the sediment deposited upstream of the mouth bar will reduce the local slope and increase friction leading to new deposits, and new avulsion. In non-cohesive channels, this cyclic morphological process will result into the autogenic fractal structure that characterizes river delta formations (Kim & Jerolmack, 2008). Therefore, the avulsion time scale exerts fundamental control on the development of a delta network and its length depends on the sediment flux and the length of the channels. The spatial and temporal scales of this cyclic formative process in river deltas have a deterministic behaviour and can be determined as function of the boundary conditions, e.g. lake level (Reitz et al.,

2010; M. Van Dijk et al., 2012). Laboratory observations have shown that when the basin presents high water level, aggradation and in-channel deposition from the mouth bar stop and channel avulsion is inhibited, leading to static distributary channels (Wang et al., 2019).

The presence of vegetation modifies the mechanism presented above for the case of non-cohesive channels by changing the time scales in which bifurcations occur and the overall delta network evolution (Piliouras & Kim, 2019). Plant roots increase sediment resistance to erosion by stabilizing alluvial bars, e.g. channel bifurcations, and reducing bank erosion, while the biomass modifies the local flow inducing sediment deposition (Nepf, 2012). For a quantitative review of this processes see Politti et al. (2018). In turn, plant dynamics are influenced by river processes that select the type and spatial distribution of riparian vegetation (Camporeale et al., 2013; Gurnell, 2014), as well as the development of the root structure (Tron et al., 2015). As a consequence, this affects the resistance offered to sediment erosion (Caponi & Siviglia, 2018) and plant uprooting by flood (Bau' et al., 2019). In addition, the interplay between vegetation growth time scales and flood occurrence control the probability of plant survival and growth (Calvani et al., 2019). In turn, this affects the collapse of vegetated banks (Corenblit et al., 2007), and so the timescale with which channels narrow or widen (Zen et al., 2016; Zen & Perona, 2020). Eventually, the interplay between plant growth and river processes determine biomass spatial distribution within the floodplain and resulting river morphological patterns (W. Van Dijk et al., 2013).

Such mutual feedback between river processes, vegetation, and basin level is ultimately controlled by changes in the climate, particularly temperature and precipitation. Moreover, the effects that changes may have on bio-morphodynamics are further enhanced in arid and semi-arid regions. The challenging environmental conditions for plant development will increase the impact that even small changes in atmospheric conditions, river flow and sediment discharge, could have on the channel morphodynamics, the type of vegetation populating the floodplain and its spatial distribution. Furthermore, high temperature could increase the evaporation rate reducing the water level within the basin receiving the river flow and sediments. Lake Turkana and the lower Omo River constitute an example of such environment, where in addition to precipitation and river flow, the lake level plays a crucial role on the control of the eco-morphodynamics of the floodplain. In a study conducted by combining early Landsat imagery and local field observations, Haack (1996) showed that the lake level had dropped around 10 m from 1973 to 1989 allowing the formation of a large wetland and an estuary at the lake inlet. An aerial survey revealed that the delta was covered predominantly by grasses on the order of 1–2 m in height, and trees and shrubs on river levees, as well as a high sediment load within the Omo River. According to the author, such high presence of sediments was generated by an increased sediment erosion in the upper part of the Omo basin due to deforestation.

Few years later, Carr (1998) described the delta area as characterized by seasonally inundated mudflats, and swamp grasslands of mixed aquatic and semiaquatic species (e.g. microphytes), with overflow from the bank typically occurring during flood season between August and September. A typical river bank within the lower Omo and the channels forming the delta presented aquatic and semiaquatic vegetation close to the water, and mesophytic grasses in the middle of the bank, while the bank crest and its downslope were covered by grassland and sparse shrubs and trees. Among the woody vegetation, the most common was, *Ficus sycomorus*, which could reach up to 15 m, but their development was prone to river overflow able to cover half of their trunk generating anoxic conditions. Because of this, the presence of woody species, as well as forest density, increased while moving upstream from the lake. For more details in the type of vegetation colonizing floodplain and channel banks of the lower Omo River, see Carr (1998).

A study conducted on a flood in 2006 showed that due to the increased intensity of local rain events associated to higher temperatures, and the augmented sediment erosion due to deforestation, floods have increased their capability to modify the floodplain by eroding banks, removing vegetation and depositing sediments. This resulted in changes of

118 the morphology of the sinuous–meandering lower reach of the Omo River, as well as the
 119 channels forming its delta (Ayalew, 2009). In addition to the changes in the local climate,
 120 the river and lake dynamics have been modified in the last decades by the construction of
 121 three dams within the Omo basin: the Gibe I, Gibe II, and Gibe III dams. Particularly,
 122 the Gibe III dam is the latest dam of the energy plan, it is 243 metres high and presents an
 123 installed power of 1,870 MW. The dam work started during 2006 and became operational in
 124 December 2016 (Avery, 2012). The effect of these dams in the surrounding environment has
 125 been source of public debate. A recently published paper analysed the filling process of the
 126 Gibe III dam, which caused a drop in the water level in Lake Turkana of 1.7 m, (Zaniolo et
 127 al., 2021). The paper provides quantitative evidence of the benefits generated by adaptive
 128 filling strategies, attaining levels of hydropower production comparable with the historical
 129 ones while curtailing the negative impacts to downstream users.

131 In this work we aim to quantify the impact of lake level changes on the eco–morphodynamics
 132 of the Omo River delta, and to seek for possible correlations to either or both climate
 133 variations and dam works. First, we aim to quantify the temporal changes in land use and
 134 atmospheric forcing occurred within the study area. Second, we analyse the historical series
 135 to assess what has induced such changes, namely: a new river hydrology imposed by the
 136 dam, or changes in the climate of the area. Third, we observe the river morphological struc-
 137 ture throughout the time frame investigated to quantify river morphodynamics and relate
 138 this to the changes mentioned above.

139 2 The study area

140 The Turkana Lake is located in the Northern–Western Kenya, at the border with
 141 Ethiopia, Africa. The lake is characterized by a long shape oriented north–south, the dis-
 142 tance between the north shore and the south shore is around 200 km and the maximum
 143 width is around 40 km. With a surface of almost 7,000 km² the Lake is the fourth largest
 144 lake in Africa and the world largest desert lake. It has a mean depth of 31 m, and a maxi-
 145 mum depth of 114 m. The lake is fed by three rivers, the Turkwel and Kerio Rivers from the
 146 South–West, and the Omo River from the North. The latter provides almost the totality
 147 of the lake inflow (90%) and flows through Ethiopia. When reaching the lake, the Omo
 148 River deposits sediments originating a branching structure (see Figure 1). The Omo River
 149 shows a humid hydrological regime with an average annual rainfall estimated around 310
 150 mm while the desert area of the Lake shows a much lower annual rate around 200 mm, which
 151 results in an average precipitation of 0.5 mm/day. Conversely, the Lake is characterized by
 152 a strong evaporation rate, which has been estimated to be around 7 mm/day (Avery, 2012).
 153 The evaporation process is enhanced by a strong South–Eastern wind, which also generates
 154 strong secondary currents that contribute to diffuse the sediments carried by the Omo River
 155 deeper into the lake and along the North–East shore.

156 The natural inflow of the Omo River is characterized by a flooding season between
 157 August and October with a maximum flow discharge of about 1,650 m³s⁻¹. Following
 158 dam operations the new river regime is characterized by two peaks occurring in May and
 159 October, which have been estimated to be around 680 m³s⁻¹ and 1,200 m³s⁻¹, respectively
 160 (see Figure 2). In addition, the modified flow presents a low flow regime, occurring during
 161 winter time and in July more than twice that of the natural flow of 200 m³s⁻¹ (Avery,
 162 2012).

163 Downstream the large bifurcation of the Omo River, the vegetation is less impacted by
 164 human activities compared to the area upstream and more regulated by the river hydrology
 165 Carr (1998). Therefore, in this work we focus on the changes associated to the delta area
 166 and surrounding shores corresponding to the upper portion of the lake as showed in Figure
 167 1, panel c). The area does not extend further upstream to avoid the inclusion in the analysis
 168 areas of the Omo floodplain characterized by cotton crop fields. Indeed, the presence of crops

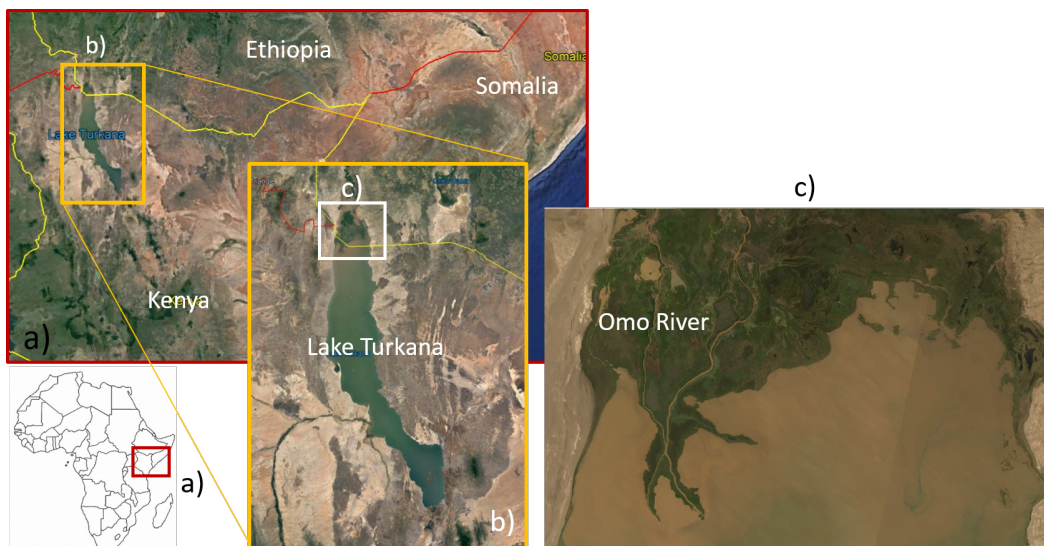


Figure 1. The study area at different zoom levels, a-c. In c), the Omo river delta clearly appears with its characteristic branching structure.

Table 1. Historical dataset used for the analysis.

Source	Type	Resolution	Interval
Landsat 5	Multispectral	30 m	1986 – 2002
Landsat 7	Multispectral	30 m	2003 – 2012
Landsat 8	Multispectral	30 m	2013 – 2019
ERA5	Reanalysis	0.1° *	1979 - present

* Spatial resolution of 9 km at the latitude of the case study.

169 will prevent a correct estimate of the spatial structure of the natural vegetation covering
170 the river floodplain and delta.

171 3 Materials and Methods

172 3.1 Historical dataset

173 A historical dataset was collected by combining data extracted from satellite imagery
174 with historical data on atmospheric variables. In particular, satellite data was used to
175 quantify spatial and temporal changes in land coverage and river/delta morphology. While
176 the historical evolution of atmospheric variables was used to assess the impact of external
177 forcing on the observed changes within the studied area. To extend the length of the time
178 frame covered, we combined different Landsat missions. Information on external forcing of
179 the ecosystem, namely, precipitation, temperature, evapotranspiration from water bodies,
180 land, and vegetation, were collected from the ERA5 dataset provided by the European
181 Centre for Medium-Range Weather Forecasts (*ECMWF*, 2021). A summary of the sources
182 used for the analysis is reported in Table 1.

183 Since the launch of the first Landsat mission in 1972 the joint program of the USGS
184 and NASA has imaged the Earth's surface twice a month, by collecting different spectral
185 bands of surface reflectance. The first four missions recorded 4 spectral bands: two bands
186 in the visible spectra, red and green, and 2 bands in the short infrared range. The more
187 recent 5, 7 and 8 missions increased the bands recorded from the satellite sensor by including
188 the blue and near infrared bands, and mission 8 also added a ultra blue band, as well as

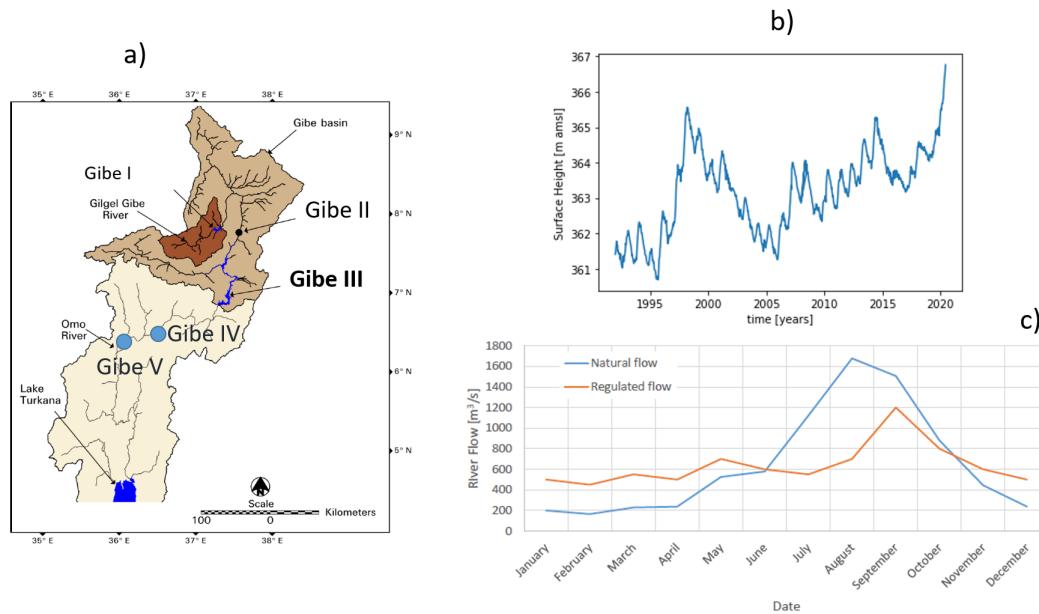


Figure 2. Frame a) shows the Omo River catchment and the location of the Gibe I, Gibe II, and Gibe III dams. The picture shows also the location of the future dams Gibe IV and Gibe V that will complete the hydroelectric development of the catchment (adapted from Avery (2012)). Frame b) depicts the water level measured from satellite altimetry. Frame c) shows the natural flow in the Omo River and flow after the Gibe III dam was built.

189 two bands associated to temperature. For the presence of the infrared band, the Landsat
 190 5 mission was the first one to allow multispectral images of the study area to be collected
 191 since 1986. Since Landsat 7 and 8 provide higher resolution both in space and time, and
 192 even more bands, we progressively collected images from more recent missions as soon as the
 193 data was available. For each image collected we used the surface reflectance atmospherically
 194 corrected product. A total of 200 images were collected covering the time interval 1986 –
 195 2019.

196 In contrast to direct satellite observations, the ERA5 (ECMWF Atmospheric Reanalysis
 197 5) dataset contains data from the reanalysis of the global climate for the European Centre
 198 for Medium-Range Weather Forecasts (ECMWF). The project combines physical-based
 199 models with observations across the world to provide high-resolved historical data available
 200 from 1979 to three months from real-time. Particularly, we used the monthly-mean values
 201 provided by the ERA5-Land dataset which focuses on land variables, including temperature,
 202 rain, snow, heat flux, evaporation, and ice (Muñoz Sabater, 2019). For this analysis, we
 203 investigated the following parameters: 2 m air temperature, precipitation, evaporation from
 204 water, bare soil, and canopy.

205 3.2 Image analysis

206 For the geo-spatial study, we analysed data available on the Google Earth Engine
 207 platform (Gorelick et al., 2017) using different Python libraries. Landsat imagery provides
 208 surface reflectance information corrected from the distortion induced by the atmosphere that
 209 generates a difference between the reflectance value measured at the top of the atmosphere
 210 and that measured at the Earth's surface. Therefore, reflectance values can be directly used
 211 to quantify the temporal evolution of the study area for each date observed.

Land Coverage

The study area was classified into four classes of land coverage, namely: water, bare ground or sediments, shrubs or young vegetation, and mature vegetation. It should be noted that the water class is then further divided into lake and river or water flooding the floodplain. This difference allowed the lake to be masked from the analysed image. In order to separate water from dry land and then quantify the portion of dry land covered by sediments or vegetation, we computed vegetation and water indices. For the first index, we used the Normalized-Difference Vegetation Index (NDVI) (Rouse et al., 1974), while for the second we adopted the Automated Water Extraction Index with No Shadow (AWEInsh) (Feyisa et al., 2014). Both indices are a linear combination of different reflectance bands and are computed as follows:

$$NDVI = \frac{\rho_4 - \rho_1}{\rho_4 + \rho_1} \quad (1)$$

$$AWEInsh = 4(\rho_2 - \rho_5) - (0.25\rho_4 + 2.75\rho_7) \quad (2)$$

where ρ_1 is the red band, ρ_2 is the green band, ρ_4 is the near infrared band, ρ_5 is the shortwave infrared band 1, and ρ_7 is the shortwave infrared band 2. Positive values of AWEInsh and NDVI are associated, respectively, to wet and dry pixels.

Among the various water indices that have been proposed in the literature, the AWEInsh index shows high efficiency in identifying mixed pixels in absence of signification elevation changes and when in the scene there are no shadows provided by mountains or buildings, nor snow (Acharya et al., 2018). Mixed pixels are typical of rivers and lake shores, where in shallow waters the presence of suspended sediments, chlorophyll or shore vegetation could lead to pixel misclassification. Once the wet land was separated from the dry land, the distribution of the positive NDVI values extracted from each pixel was obtained for each available date. This allowed us to compute the principal moments of the distributions, obtaining a value of mean, variance, and skewness for each collected images of the dataset.

The typical distribution of NDVI values, for the study area, is a multimodal distribution with three peaks. Therefore, we classified the dry land portion into bare ground, shrubs or young vegetation and mature vegetation, considering that mature canopy presents more foliage and thus higher NDVI values. In a study conducted on a riparian environment in the temperate zone, Henshaw et al. (2013) identified NDVI values lower than 0.2 with bare ground and greater with vegetation. Another study conducted over a period of 13 years on different types of vegetation for a north-Africa semi-arid region Amri et al. (2011) observed that, on average, NDVI values were comprises between 0.2 and 0.4 for shrubs, pastures and sparse small trees, with extreme seasonal values ranging between 0.2 and 0.5. An analysis on the efficacy of vegetation optical depth to estimate vegetation green biomass in African drylands presented an NDVI in the range 0.2-0.5 for low values of biomass that progressively increased when biomass increases. Particularly, when woody canopy occupied more than 10% of the study area the NDVI values where higher than 0.4 (Tian et al., 2016). By considering these values, a pixel was classified as bare ground when $0 \leq NDVI < 0.2$, shrubs if $0.2 \leq NDVI < 0.4$, and mature vegetation when $NDVI \geq 0.4$.

Because wet sediments can be detected as water when analysing multispectral imagery, water and bare ground classes were joined together in order to compare different land coverage in the signal analysis. Few preliminary operations were required before analysing the satellite imagery. Due to a failure of Landsat 7's Scan Line Corrector, since 2003 Landsat 7 images were not collected following a straight path but a zigzag path, which resulted in the black stripes of missing data characterizing images from Landsat 7 (*USGS-Landsat7*, 2021). Therefore, a 5-pixel square window was moved around the whole image and the median of the neighbours was assigned to the central pixel. The original image was then superimposed on top of the filtered one to keep the resolution of the original image where possible. Finally,

259 images presenting a cloud coverage value greater than 5% were rejected at the beginning of
260 the analysis.

261 *River morphology*

262 Changes in river and lake delta morphology throughout the time frame considered in
263 the analysis were analyzed. First, the lake was masked from the image on the base of
264 the AWEInsh value, leaving the shore and the river because of their shallow water (which
265 generated lower values of AWEInsh). Second, a combination of the AWEInsh and NDVI
266 were applied to the new masked image to extract a binary image of the river, i.e. pixel
267 values 0 and 1 were associated to land and water, respectively. Third, the binary image
268 obtained was analysed by using morphological operations (e.g. erosion, dilation) to get rid
269 of wet portion of land and further isolate the river structure. Once the river structure was
270 available, the number of bifurcations from the main channels were computed as proxy of
271 morphological activity. In this count, we included any bifurcation within the main channels
272 as well as river branches associated to an anastomized pattern and those characterizing the
273 fractal structure of the river delta. However, due to difficulties in completely removing wet
274 areas close to branches of the Omo River, the counting operation was made manually, once
275 the river structure was clearly outlined.

276 **3.3 Time series analysis**

277 The historical time series of land coverage and climate variables were analysed to explore
278 relationships between changes in land coverage, amount of precipitations, air temperature,
279 and evaporation rate. Before doing this, a preliminary operation was required to re-sample
280 all the signals to the same one-month time interval. Because data extracted from Landsat
281 missions did not allow a constant sampling frequency, the signal extracted from the analysis
282 of the multi spectral imagery was interpolated using splines interpolation and data was
283 re-sampled using a monthly time interval, in order to match the same time resolution of
284 the ERA5 dataset. Such newly generated signals were then used to explore changes in the
285 period before and after the construction of the dam began. Since the works to built the
286 dam started during 2006, we chose the 1st January 2007 as a date from which dam building
287 operations could have impacted the water and sediment dynamics in the downstream river
288 reach and its floodplain. A further comment is however in order here. Following the start
289 of the construction works in 2007, the dam became operational only many years later. As a
290 consequence, the results of our analyses for the "postdam" period will actually be damped
291 by the inclusion of the time series recorded during the construction time.

292 A Fourier analysis was conducted on the one-month resolution signals and the first five
293 frequencies characterized by higher power spectrum were used to low-pass filter the series.
294 The filtered signal, almost deseasonalized, was assumed to be representative of the trend.
295 In order to perform this analysis each signal was repeated 20 times to introduce periodicity
296 and obtain a long time series more suitable for the Fourier analysis. The auto-correlation
297 function was computed for all the land coverage signals, before and after the Gibe III dam,
298 to quantify temporal changes associated to the presence of the dam. Since low frequencies,
299 i.e. seasonality, temporary induced correlation within the signal, the original signal was
300 filtered by keeping only the higher frequencies. This was achieved by subtracting the long
301 term trend obtained through the Fourier analysis to the original signal.

302 Because changes in land coverage may be associated also to changes in weather condi-
303 tions, we compared the time evolution of land cover with that of the atmospheric variables.
304 First, we computed the annual minimum, mean, and maximum of air temperature, evapora-
305 tion from sediments and evaporation from vegetation. Second, the cross-correlation function
306 was computed for the following couple of detrended signals: shrubs and water, mature veg-
307 etation and water, shrubs and temperature, and mature vegetation and temperature. By
308 considering that sediment and water coverage are mutually dependent, i.e. if water increases

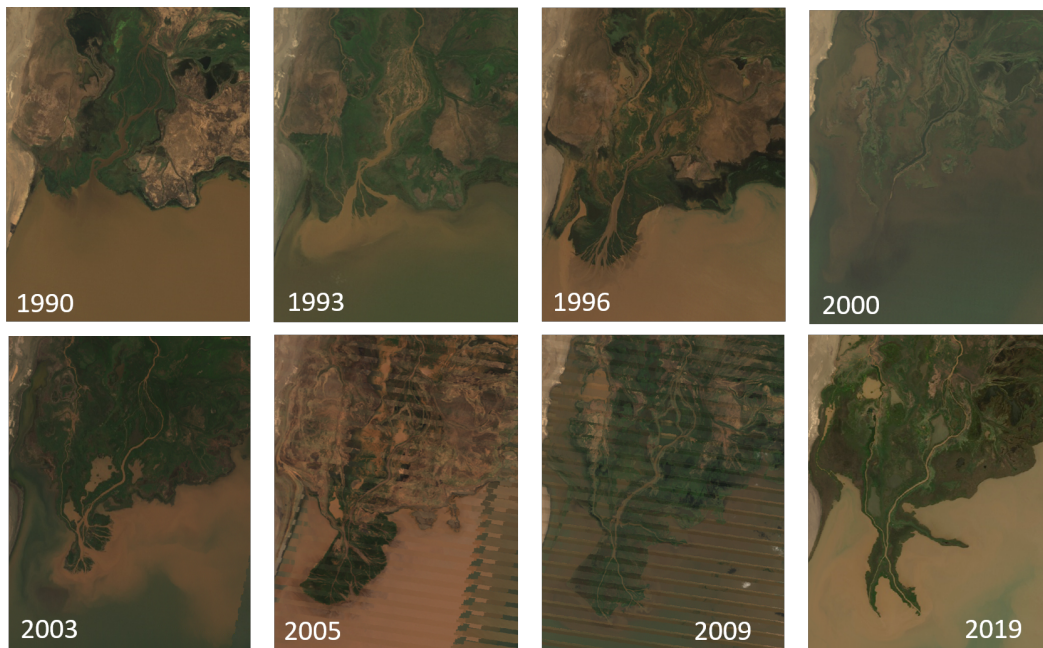


Figure 3. Historical sequence showing the evolution of the study area as observed from satellite imagery.

309 dry sediment portion decreases and vice versa, in computing the cross-correlation function,
 310 water and bare ground time signals were combined together. Henceforth, we will refer to
 311 this combined signal as to the non-vegetated signal.

312 A linear correlation analysis was conducted on the detrended signal. This would allow
 313 to assess the level of noise affecting the series and then upon occurrence to remove it by
 314 using, for example, autoregressive models (Głogowski et al., 2021). However, this operation
 315 was done only for those variables sampled with sufficient high resolution, e.g. like the
 316 environmental ones. Finally, in order to compare different variables, all the detrended
 317 signals were preliminary standardised, by subtracting their mean and dividing the result for
 318 their standard deviation.

319 4 Results

320 Figure 3 shows a discrete temporal sequence of satellite images of the domain being
 321 studied. To notice, are the early formation of the delta in 1993, and its subsequent develop-
 322 ment until the period of high water level (panel related to year 2000 in Figure 3) as seen in
 323 Figure 2b. After shore and floodplain were flooded, the river modified its course and delta
 324 structure (years 2003, 2005 in Figure 3). Later, a less complex delta structure appeared,
 325 and the river presented an almost single thread channel upstream, with an anastomosing
 326 section and a bifurcation before reaching its delta, which at this stage was reduced to two
 327 main channels (year 2009 in Figure 3). The latter channel morphology is kept unchanged in
 328 the following years, while a substantial erosion of the sediments forming the delta occurred
 329 (year 2018). The diagonal lines in the panels associated to year 2005 and 2009 are the result
 330 of the interpolation conducted to fill the stripes with no data due to a malfunctioning of the
 331 sensor on board of the Landsat 7 mission.

332 The multispectral imagery, of which their RGB (Red-Green-Blue, or visible) bands
 333 combination is presented in Figure 3, were used to estimate the water and vegetation index,

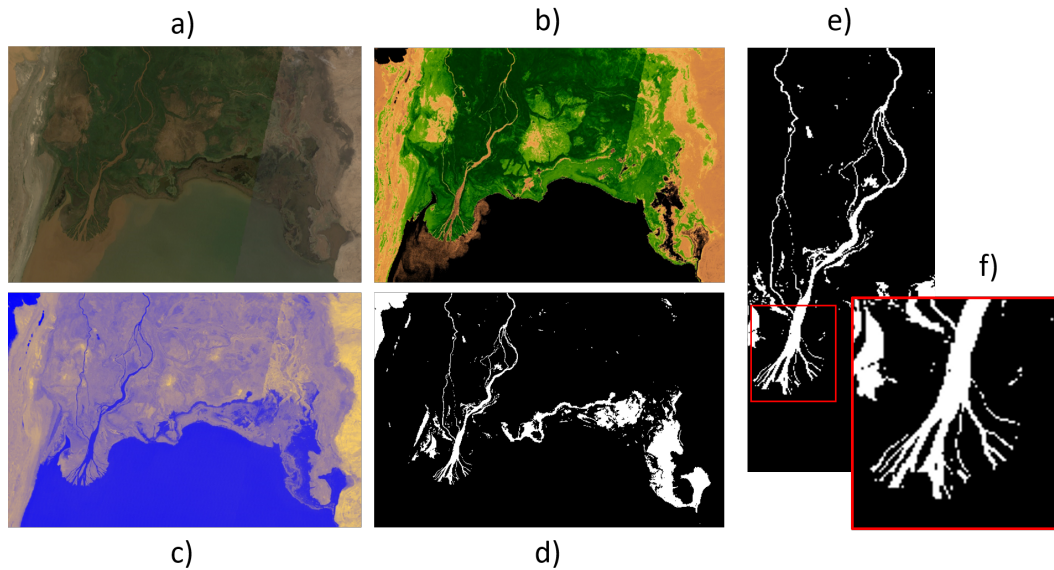


Figure 4. Example of the image analysis conducted for the study area. a) RGB image, b) NDVI, c) AWEInsh, d) lake waters masked from the wet portion, e) river structure, and f) close up showing the details of the delta morphology.

334 AWEInsh and NDVI, respectively. These two indexes were used to assess the land cover
 335 type for the different dates available, and to separate the Omo river from the Turkana Lake.
 336 An example of the image analysis conducted is reported in Figure 4. Figure 4a shows the
 337 RGB image. Figure 4b and c show the distribution of the NDVI and AWEInsh values,
 338 respectively. Colours in Figure 4b go from 0 to 1, such that pixels below or equal to 0
 339 appear black. Although these values are usually associated to water, it can be noticed that
 340 in Figure 4b the Omo river and the delta area do not appear black. This is essentially due
 341 to the presence of suspended sediments and macrophytes within the Omo River that induce
 342 higher reflectance of the NIR (Near-Infra-Red) spectrum compared to that observed for
 343 clear water. This is also supported by the diffusion observed around the delta, indicating
 344 the release of solid transport from the river to the lake, compared to the sharp border
 345 identified in the AWEInsh image (Figure 4c). This latter index allows to clearly identify
 346 the lake border and the main channel of the Omo River, but barely detect the presence of
 347 secondary channels in the anastomosed section. Therefore, AWEInsh was used to mask the
 348 portion of the study area covered by the lake, and a combination of the NDVI values with
 349 AWEInsh values was used to extract the morphology of the channel as reported in Figures
 350 4d, e, and f.

351 The analysis of satellite imagery allows to quantify spatial and temporal changes in land
 352 coverage and the results were presented as percentage of the study area. Such results are
 353 reported in Figure 5a-d along with the other historical series for precipitation (Figure 5e),
 354 temperature (Figure 5f), evaporation from water (Figure 5g), evaporation from bare soil
 355 (Figure 5h), and evaporation from vegetation (Figure 5i), that were collected from ERA5
 356 dataset. Each panel presents in blue the original signal and in orange the long term signal
 357 filtered from the higher frequencies. Time signals that describe the evolution of system
 358 variable in natural systems are characterized by a medium-long term trend and short-term
 359 events. Therefore, each signal can be decomposed into a deterministic and a stochastic
 360 component. The long-term component of each analyzed signal is reported in orange in
 361 Figure 5. The filtered signal shows the Fourier series of the first five modes characterized by

362 highest power spectrum. Such signal represent the seasonality of the variable. The analysis
 363 highlights a progressive rise in air temperature since the year 2000 and an increase in the
 364 evaporation from the vegetative compartment since the year 2008. After 2006, water coverage
 365 shows an increasing trend, opposite to sediment and young vegetation that progressively
 366 decrease, with the study area showing almost no bare ground spots by the end of the time
 367 period analysed. Conversely, mature vegetation shows an almost constant trend after 2008.

368 Around 1997 an increase in the annual rainfall of about 380mm/yr (Avery, 2011) de-
 369 termined a high water level in the lake and the Omo River, with consequent overflow and
 370 inundation of a great portion of the study area (see Figure 5d). After this event the rain
 371 events showed an increasing trend, which possibly kept a high level within the river and
 372 lake (Avery, 2011). This induced an abrupt diminishing in vegetation, for both classes, as
 373 well as for the dry bare ground area (see Figure 5 b,c,d). However, while the amount of ex-
 374 posed sediments recovered fairly immediately to its original value, both shrubs and mature
 375 vegetation required a long time to recover to their previous condition. It should be noted
 376 that such recovery trend is inverted for shrubs around 2007 without allowing this vegetation
 377 type to recover to the same area occupied in the early 1990s before the inundation period
 378 took place. On the other hand, mature canopy recovered to its previous status, which it
 379 kept almost constant after 2007. The amount of exposed sediments keep oscillating until
 380 around 2008 when the portion of dry bare ground start to decrease until almost completely
 381 disappearing. The portion of land lost by shrubs and dry sediments seems to be substituted
 382 by water and mature vegetation.

383 The analysis of the historical trend for the environmental variables extracted from
 384 the ERA5 dataset, namely air temperature, and evaporation from soil and vegetation, are
 385 reported in panels e), f), g), h), i) of Figure 5. These data show an increase in air temperature
 386 after 2003, while the evaporation from wet surface remain unchanged over time. The amount
 387 of water evaporating from the soil surface shows a medium-long term signal with a regular
 388 pattern and a frequency of about 5 years, as well as high frequencies with values progressively
 389 decreasing after 2006. On the other hand, the medium-long term signal of the evaporation
 390 from vegetation shows a frequency of about 3 years, while the high frequencies present values
 391 that slightly increase after 2006.

392 This behaviour is better shown in Figure 6, where the yearly minimum, maximum, and
 393 average values are presented for air temperature, evaporation from soil, and evaporation from
 394 vegetation in Figures 6a, b, and c, respectively. The average annual temperature presented
 395 an oscillatory pattern with a frequency of 10 years until 2003, and an almost constant value
 396 around 29°C after. This is possibly due to a combination of the high maximum temperatures
 397 recorded between 2007 and 2009, and the high minimum temperatures observed between
 398 2009 and 2015, of about 29°C. The average annual value of the water evaporated from the
 399 canopy followed the temperature pattern, with the same 10-year oscillations: maximum
 400 and minimum values around 1986 and 1996, and 1991 and 2001, respectively (see Figure
 401 6c). After 2003, the oscillations are minimal and the average evaporation from trees was
 402 around $3.5 \cdot 10^{-3}$ m. Also in this case, there was a consistent increase in the minimum annual
 403 evaporation after 2003. Conversely, the annual average of water evaporated from the bare
 404 soil was not aligned with the air temperature trend (Figure 6b). First, the values before 2003
 405 are anti correlated with those of temperature. Second, the average values decreased between
 406 2006 and 2011 to a value of $0.5 \cdot 10^{-4}$ m, and started to oscillate around an evaporation of 0.6
 407 10^{-4} m with a frequency of 5 years. This decreasing trend is also evident in the maximum
 408 annual values, while the minimum values of evaporation remained almost constant trough
 409 the time frame explored.

410 All time series were split into two signals before and after the start of the construction
 411 works of the dam, whose reference date was chosen to be 1st January 2007. The autocorre-
 412 lation function was performed on the detrended signals. Results are reported in Figure 7 for
 413 the land coverage signals before (blue line) and after (red line) the start of the works. All

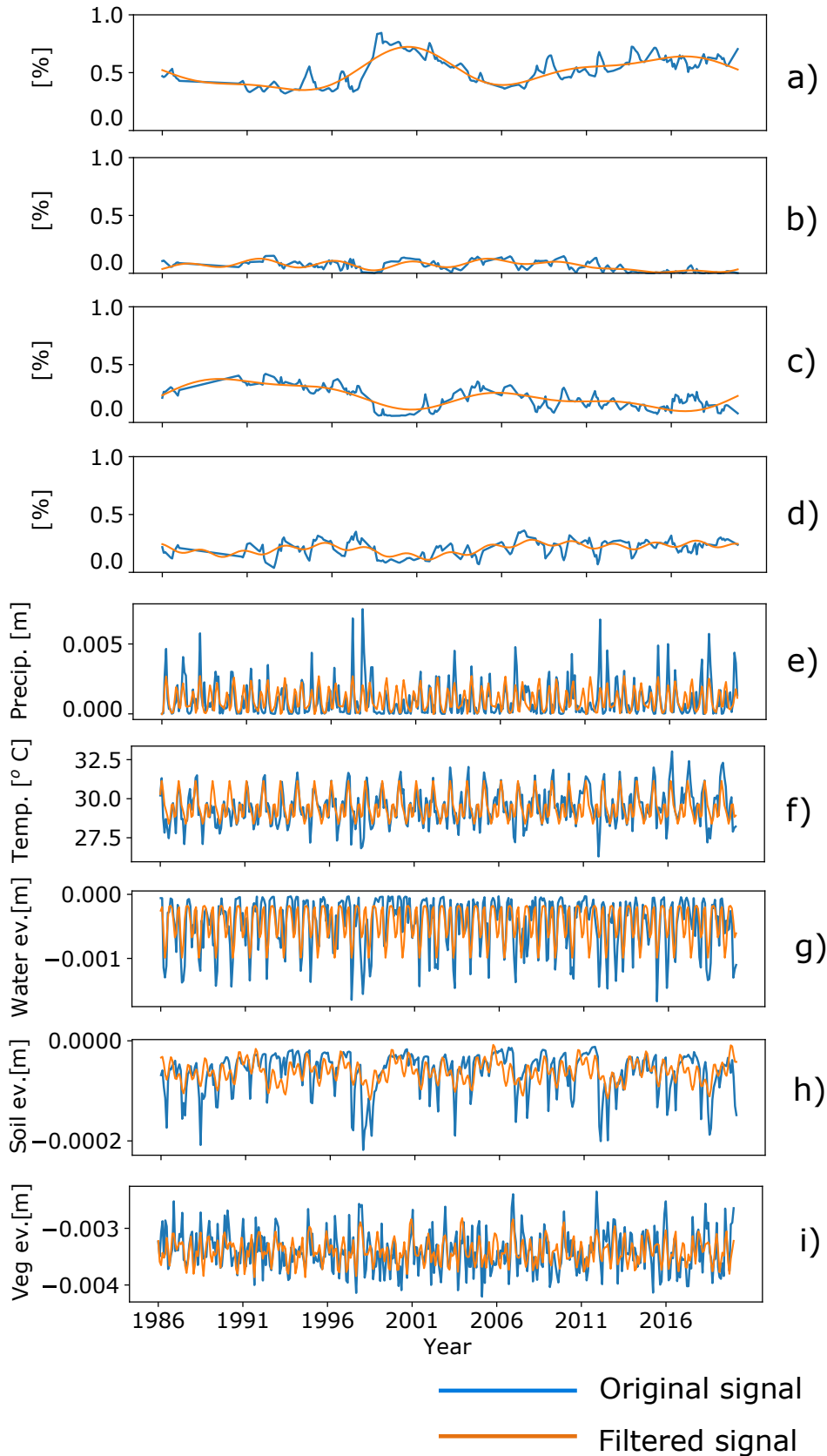


Figure 5. Historical series of land coverage and atmospheric variables extracted from satellite data for the time period 1984-2019. Blue and orange line indicate original and filtered signal, respectively. Panels a-d present changes in land coverage within the study area observed by combining images of Landsat 5,7 and 8, with a) showing the wet land, and the dried land divided into b) bare ground, c) shrubs or juvenile vegetation, and d) mature vegetation. Panels e-i show the time series extracted from ERA5 data for the study area: e) precipitation (m), f) temperature (°C), and g), h) and i) the cumulative amount of water evaporated in one month from water, bare ground, and vegetation.

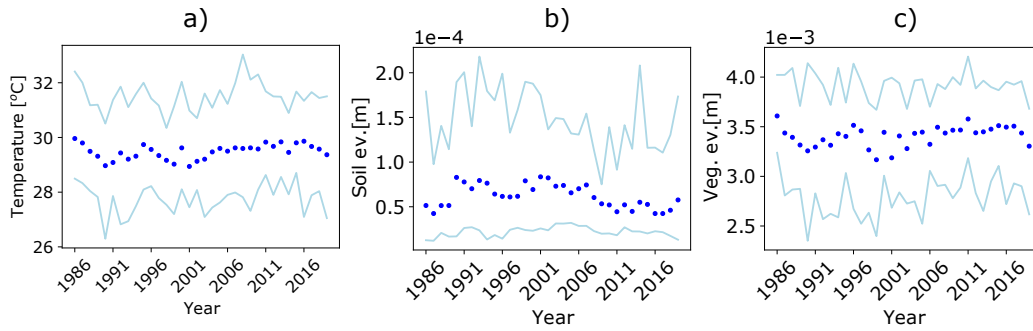


Figure 6. Annual average (dotted line), minimum and maximum (solid lines) for a) air temperature, b) evaporation from bare soil, and c) evaporation from canopy.

414 the autocorrelation functions reported in Figure 7 show a structure representing a temporal
 415 correlation that operates at annual and seasonal time scales.

416 Panel a) of Figure 7 shows no changes between the two periods, while b) and d) show
 417 that, respectively, the signals for sediments and mature vegetation lost correlation after the
 418 starting of the construction works, with the dynamics of the bar ground surface presenting
 419 a lag shift of almost 5 months between the pre- and post-dam scenarios. Likely, this earlier
 420 decorrelation of the bare ground surface explains the appearance of a peak of annual cor-
 421 relation in young vegetation in the post-dam period (Figure 7 c). Accordingly, shrubs and
 422 mature vegetation showed changes in their autocorrelation structure before and after the
 423 construction of the dam (Figure 7c and d), but the average temperature of the area also
 424 increased during a very similar period (see Figure 6a) and may have influenced these two
 425 dynamics as well.

426 Vegetation dynamics could have been impacted by changes in fluvial processes, i.e.
 427 river flow and sediment load, due to the construction and operation of the dam, but also by
 428 variations in temperature (Figure 6a). For this reasons, time series associated to vegetation
 429 type were compared with the non-vegetated signal (sediment and water) and temperature
 430 time series. Figure 8 shows the cross-correlation function for the following couple of vari-
 431 ables: non-vegetated and young vegetation (Figure 8), non-vegetated and mature vegetation
 432 (Figure 8b), temperature and young vegetation (Figure 8c), and temperature and mature
 433 vegetation (Figure 8d). As for the autocorrelation function above, also the cross-correlation
 434 function was computed for the period before and after the dam construction.

435 Panels a and b of Figure 8 show that vegetation is inversely related to changes in water
 436 and sediment. Although water and sediment signals are combined, the changes in water
 437 coverage have a dominant effect in controlling the overall trend of the combined signal.
 438 This means that when water level increases vegetation decreases. However, this behaviour
 439 is modified after the dam was built, with the two signals being correlated for half of the time
 440 they were previously correlated. Figure 8 c and d show that the cross-correlation function
 441 between vegetation coverage and temperature also presents a structure. This means that the
 442 monthly resolution with which data are available introduce a within-signal correlation that
 443 operates at the time scale of one year. Although, from 2003 the average temperature has
 444 increased (Figure 6a), the cross-correlation functions between vegetation and temperature
 445 did not change before and after the dam (2007).

446 Further investigations on land coverage changes were conducted by analysing the tem-
 447 poral evolution of NDVI values. The analysis of the distribution of NDVI values within the
 448 study area per each date observed revealed an increasing average after the dam was built

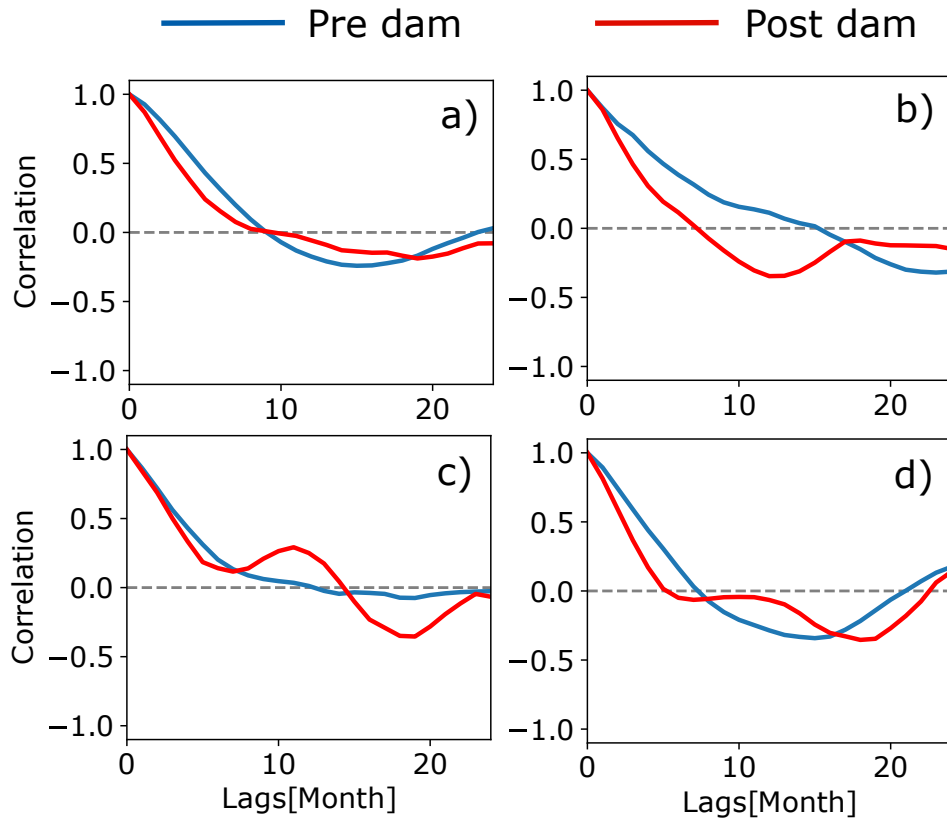


Figure 7. Autocorrelation function for the land coverage signals a) water, b) bare ground, c) shrubs, and d) mature vegetation; for the period before and after the Gibe III dam was initially built reported in blue and red, respectively.

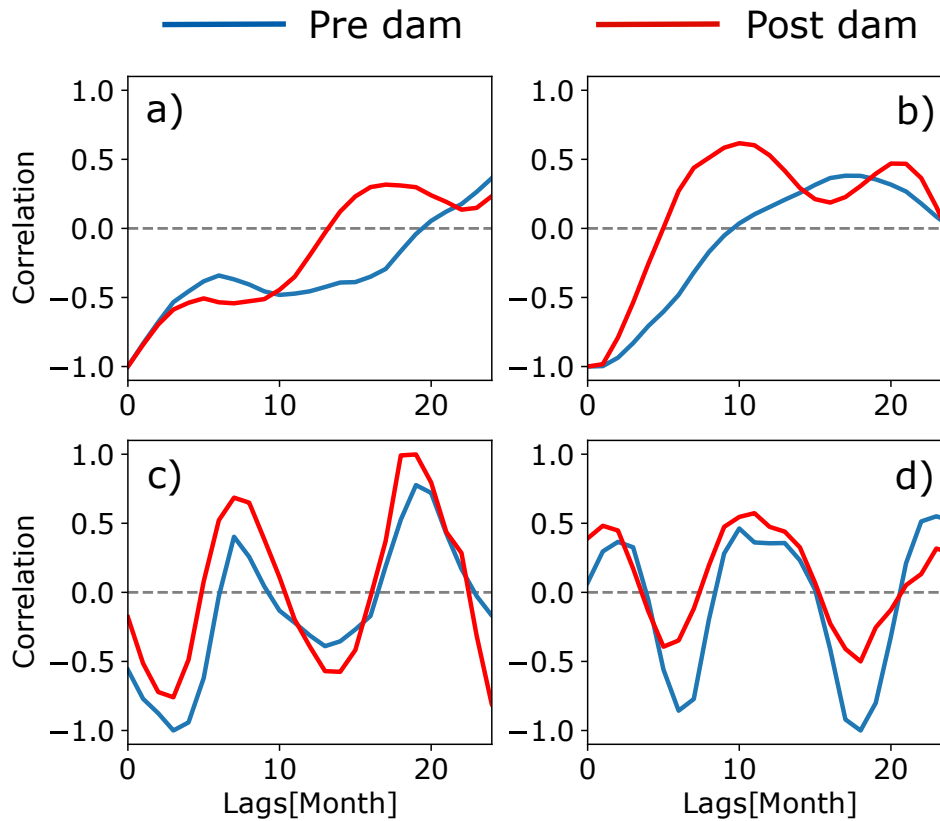


Figure 8. Cross-correlation function for the land coverage signals a) sediment water and shrubs, b) sediment and water and mature vegetation, c) temperature and shrubs, and d) temperature and mature vegetation; for the period before and after the Gibe III dam was initially built reported in blue and red, respectively.

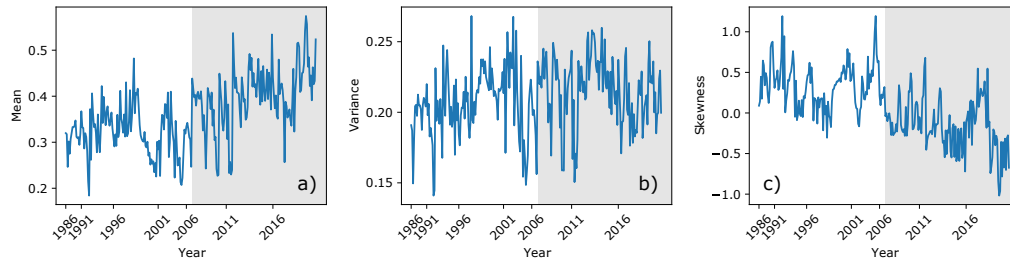


Figure 9. Major statistics of the NDVI values distribution for the dates images were available. Shadow background indicates the presence of the dam (construction started in 2007).

449 (Figure 9a). More interesting are the results obtained for the third moment of the NDVI
 450 distribution, which shows how the vegetation distribution has been progressively skewed
 451 toward mature vegetation after the dam was built, i.e. negative skewed. Nevertheless, the
 452 variance values for the same distributions have not changed during the time frame consid-
 453 ered in the analysis. This means that young vegetation persist in the study area even after
 454 the construction of the dam, but it saw the portion of land occupied shrinking after 2007.

455 Figure 10 presents the morphological evolution of the river and its delta through the
 456 time period considered in the analysis (panels of Figure 10a and close ups on Figure 10b).
 457 Panel c shows the value of the morphological index, which indicates the number of bifur-
 458 cations observed for the river segment and delta within the study area. Figure 10 clearly
 459 shows how after the construction of the dam in 2007 (gray shade in the plot) the river
 460 progressively diminished the complexity of its morphological structures both as number and
 461 variability in time. Before the dam was built, the river was highly dynamic with a lot of
 462 secondary branches that were destroyed and generated during floods. This is supported by
 463 the variations observed in Figure 10c before year 2007. In this pre-dam phase, the abrupt
 464 decrease in number of channels is associated to an increase in the lake level that overflow
 465 the floodplain for few years as it can be seen in Figure 5a. The post-dam period (grey
 466 background in the plot) is characterized by smaller variations in the number of channels
 467 with a channel hyper simplified and almost unable to evolve after 2016 (i.e. almost constant
 468 3 bifurcations).

469 5 Discussion and conclusion

470 5.1 Changes in climate variables and boundary conditions

471 Figure 5e shows an increasing frequency in large rain events after 2009. This may
 472 have lead to a higher flow in the Omo River and, consequently, to a deeper lake level, as
 473 suggested also from the positive trend of the percentage of wet study area (Figure 5a).
 474 Measurements of lake level from satellite altimeter (USGS) revealed that the lake level has
 475 constantly increased after the dam became operational in 2016. Indeed, the hydrograph in
 476 Figure 5e shows how the dam released in the lake a larger discharge compared to the natural
 477 one for the majority of the year. However, simulations conducted to explore the impact of
 478 the Gibe III dam have revealed that the increase in water level observed within the last
 479 decades is less than the rise that the lake would have experienced if fed by a natural inflow.
 480 Nevertheless, the level rise may have hampered the deposit and avulsion cycle that guides
 481 delta development (Wang et al., 2019), since the delta first originated during a much lower
 482 level of the lake in the 1970s (Haack, 1996).

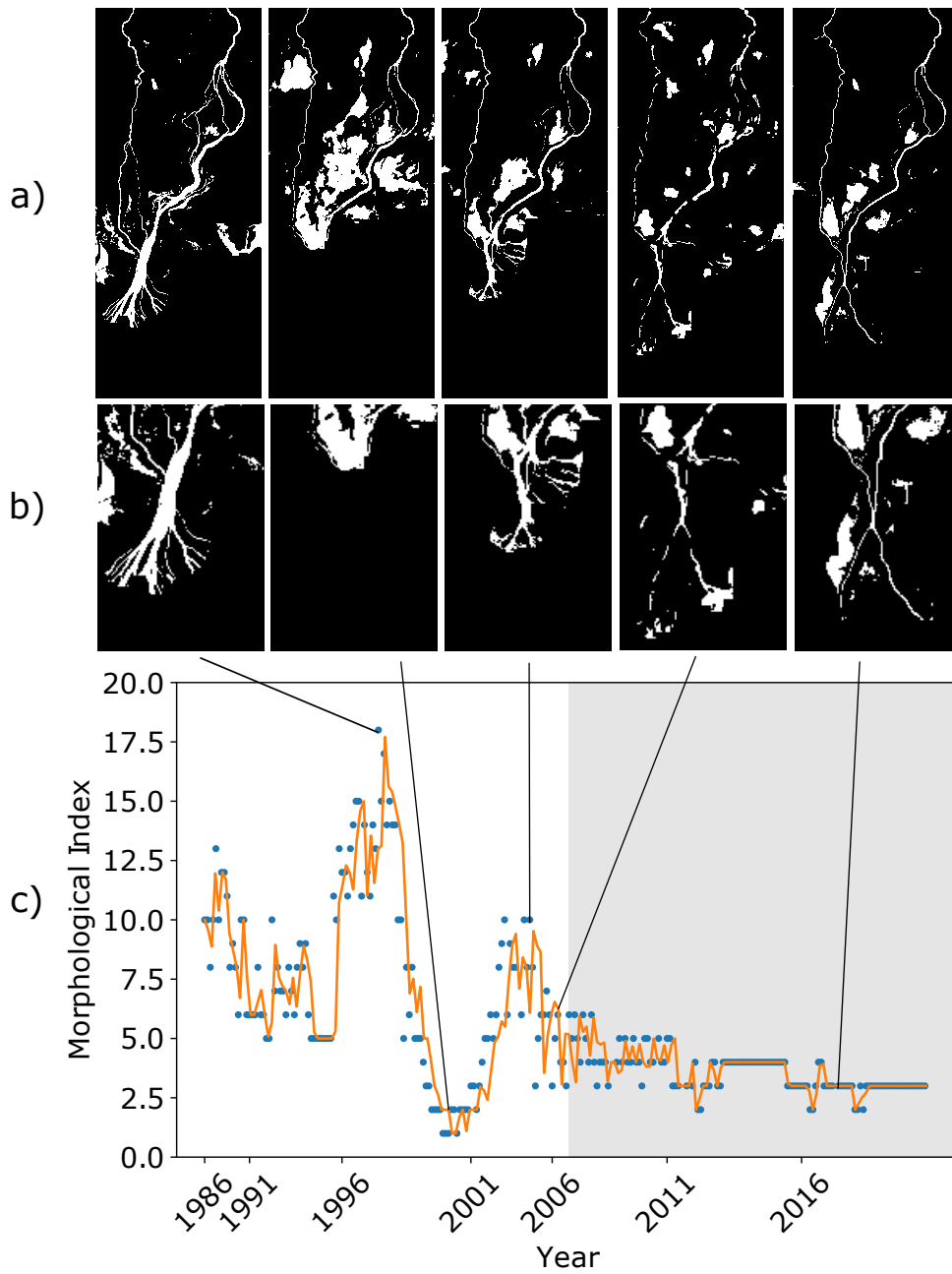


Figure 10. River morphodynamics of the lower reach of the Omo River as observed from the satellite images. Panels show a) the lower reach of the Omo River, b) a close up with the detail of the delta structure, and c) the temporal evolution of the river planform where the number of bifurcations, i.e. morphological index, is used as proxy of morphological processes.

483 The rise in the annual minimum and average temperature after 2003 (Figure 6a) is
484 associated to a decrease and increase of the evaporation recorded from the bare soil (Figure
485 6b) and vegetation (Figure 6c), respectively. While the former is due to a reduced amount
486 of dry bare sediments, the increase in evaporation from vegetation could be given by the
487 increase in temperature observed. The cross-correlation function computed for the couple
488 vegetation-temperature for the period before and after the dam revealed no changes in the
489 cross-correlation structure (Figure 8c and d). By considering that changes in air temperature
490 were observed starting from 2003 and the after-dam period started in 2007, we can argue that
491 temperature may have increased the evaporation from vegetation, but it was not responsible
492 for changes in vegetation dynamics.

493 5.2 River and delta morphodynamics

494 The morphology of the lower reach of the Omo River has experienced large changes
495 within the past 50 years (Haack, 1996). The historical dataset collected in this analy-
496 sis showed how the river was morphologically active with an anastomosing pattern in the
497 sinuous-meandering reach and a delta characterized by the typical fractal structure Figure
498 3). The planform evolution and the continuous abandonment and activation of channels in
499 the upstream sections of the study area were the result of a natural river flow that, dur-
500 ing floods, was able to erode banks and deposit sediments over the river banks or along
501 the channel where flow velocity locally decreased or secondary currents generated. This
502 promoted channel bifurcations and allowed the deposition of mouth bars that, in turn, trig-
503 gered channel avulsion generating the delta structure. Figure 5a,b and e showed that the
504 increase in the area covered by bare sediments (Figure 5b) occurred after large rain events
505 that increased the portion of wet study area (see Figure 5a, and e). This suggested that the
506 rise in the portion of dry land covered by bare sediments was due to water retreating after
507 floods and new sediments deposited during the flood that locally modified the floodplain
508 topography.

509 Sediment deposition generated mouth bars and bifurcated the main channel, or in the
510 case that a bifurcation already existed, it backfilled the channel and generated avulsion
511 upstream, widening the bifurcation. However, this cyclic process is also controlled by the
512 downstream boundary condition imposed by the lake level. It should be noted how after
513 the highest level experienced by the lake within the investigated time frame, the Omo
514 River presented almost half of the bifurcations observed in the channel in 1998 (see Figure
515 10). The number of channels remained low in the following years and the water coverage
516 presented an increasing trend. In 2001 the number of distributary channels or bifurcations
517 observed were very low due to the high level of the lake that did not allow the channels to be
518 seen from satellite imagery. During the following five years, the number of bifurcations had
519 progressively increased reaching a value of 10 as before the lake rose flooding the floodplain.
520 Then, in one year, the channel bifurcations observed dropped to 5. After this, the river
521 started to oscillate between 3 and 6 bifurcations. This diminished number of bifurcations
522 was probably caused by the increase in the lake level that hampered the delta formation
523 mechanism (Wang et al., 2019).

524 After the works to build the dam started, we observed a further decrease in the number
525 of channels, with the delta morphology limited to one major bifurcation after 2012. It is
526 reasonable to assume that this abrupt change in river morphodynamics is due to the reduced
527 sediment load available for the river downstream the Gibe III dam. In particular, the impact
528 of the lack of sediments for the river was threefold. First, to limit the deposition of mouth-
529 bar and the channel backfilling mechanisms at the base of the formation of deltas. Second,
530 to increase the erosion of the channel bed, which in turn reduces channel avulsion, and
531 progressively disconnect the channel from its floodplain. Third, to reduce the average delta
532 elevation via sediment erosion, further enhancing the effect associated to lake level rising
533 discussed above. This latter phenomena is supported by the evolution of bare sediments
534 coverage (Figure 3b). This is also evident from the autocorrelation function computed for

535 the bare ground signal before and after the dam was built (7b). The function showed that
 536 the autocorrelation time halved from 16 to 8 months, reaching a frequency close to that
 537 of the water coverage (7a). This means that, after the dam, the possibility to see dry or
 538 wet sediments from the image was directly associated to the water coverage. Such that
 539 sediments were exposed and visible during low river flow and low lake level, and submerged
 540 during and after floods or high lake levels.

541 It is possible that, before the works for the dam, the complex morphological structures
 542 and river morphology that characterized the study area provided preferential way for the
 543 overflow from either lake and river keeping large amounts of sediments exposed regardless
 544 the water depth. Finally, different temporal scales of the bare ground signal (Figure 7b)
 545 could be associated to the fact that in a more natural system, i.e. before the dam, more
 546 floods were required to rework the floodplain and the channel itself changing the sediment
 547 deposition pattern. This concept is, however, directly influenced by vegetation dynamics,
 548 since plants are able to increase the resistance to sediment erosion. In order to remove a
 549 vegetated sediment deposit, the magnitude of the flood needs to be larger than the one that
 550 generated the deposit, of a quantity which is proportional to the plant stage of development
 551 (Corenblit et al., 2007).

552 **5.3 Vegetation dynamics and interaction with river and lake processes**

553 The analysis revealed that changes in vegetation distribution have accompanied the
 554 heavy morphological evolution of the river. The autocorrelation function computed for
 555 both dense and sparse vegetation biomass presented the same frequency of water before the
 556 dam was built. This means that, during floods either or both river and lake side vegetation
 557 were killed, removed or damaged. Evidence of this can be appreciated in the historical
 558 signal of Figure 5c and d, where rain events (Figure 5e) or increases in water coverage
 559 (Figure 5a) are associated to a decrease in vegetation biomass. This variation is more
 560 evident in sparse vegetation biomass than for dense vegetation biomass. We could explain
 561 this behaviour by recalling that plant clusters provide self-protection to plants by reducing
 562 the drag and channel bed erosion (Nepf, 2012). Single stands growing at the top of the river
 563 banks or shrubs populating the mudflat (Carr, 1998) would be easily uprooted during
 564 floods, experience anoxic conditions related to high water depth or because they are buried
 565 by sediments. After the dam was built, the signal associated to sparse vegetation biomass
 566 increased the correlation on almost 6 months. Dense vegetation reduced its autocorrelation
 567 on few months but after that, the function remained null for almost a year, meaning that
 568 part of the recent signal showed no correlation, i.e. white noise. Changes in vegetation
 569 coverage associated to the disturbance generated by the dam will require longer time scales,
 570 will affect also sparse vegetation, and will not show a random pattern. Therefore, it is
 571 possible that the random changes in dense vegetation biomass observed were caused by
 572 small fires lightened by local people to free some space for cattle activities.

573 We investigated the impact that changes in local temperature and water level could
 574 have had on the vegetation. We showed that higher air temperature (Figure 6a) did not
 575 affect vegetation dynamics since no major changes were observed in the cross-correlation
 576 functions (Figure 8c and d). It is interesting to notice though that air temperature is
 577 anticorrelated with sparse vegetation biomass compared with dense vegetation biomass.
 578 This can be associated with a higher stress provided to isolated stand or shrubs by an
 579 increase in temperature, particularly in arid or semi-arid environments, compared to dense
 580 vegetation biomass that can mitigate the effect of temperature on the evapotranspiration
 581 rate.

582 More interesting are the cross-correlation functions obtained for the two type of veg-
 583 etation biomass and changes in wet surface (i.e. bare ground plus water). The signals
 584 are obviously anticorrelated and show a major change in their time scales before and after
 585 the dam was built. Both sparse and dense vegetation reduced the time lag for which they

586 are correlated with the variation of sediments and water by almost half (Figure 8a and b).
587 In addition, since 2016 the dam controls the river flow that present two peaks per year,
588 compared to the only peak experienced during the flood season per year. This may have
589 influenced the signal, although it had an impact on a limited portion of it. The reduced
590 time in which vegetation becomes correlated with water variations means that the higher
591 and almost constant low flow provides a more suitable environment for plants (e.g. higher
592 and constant water table) that grow faster. Field observations associated the low presence
593 of plants along the river with the high seasonal fluctuations of soil moisture. After the dam,
594 the controlled flow shortened the flood season and reduced floods magnitude by limiting the
595 possibility of flood to remove vegetation via uprooting or anoxic conditions. Plants are even
596 more protected by a probably incised channel that further reduces the chances of overflow.
597 The fact that less plants are removed or die during floods is also supported by the lack of
598 bare sediments observed in Figure 5b.

599 As a results, the vegetation biomass distribution has changed, which is evident from
600 the temporal evolution of the statistics computed for the NDVI distribution (Figure 9). The
601 values, particularly the kurtosis, revealed that after the dam was built the local vegetation
602 tends to present more dense biomass (high values of NDVI) compared to the scenario before
603 the dam where vegetation biomass appeared well distributed between sparse and dense. It
604 is however unclear whether existing vegetation types are more diffused due to changes in
605 river and floodplain morphodynamics or new alien species have colonized the study area
606 along with the existing ones. To the best of our knowledge, no studies have been conducted
607 with the detail of the investigation performed by (Carr, 1998), which could shed light on
608 this evolution in the vegetation coverage.

609 Finally, a remark should be added on the use of the NDVI in this work, since NDVI
610 depends on the time of the year the image was taken, e.g. plant vegetative state. Because
611 of this, the comparison between two different dates may lead to misinterpretations on the
612 evolution of vegetation within the study area. In order to get rid of this uncertainty, in our
613 analysis we referred to the long term trend by investigating the time signals for vegetation
614 coverage and the long term evolution of the statistics of the NDVI distribution within the
615 study area. Figure 11 shows a schematic of the different probability distribution of the
616 NDVI values for the study area that characterizes the time period before and after the dam.

617 **5.4 Conceptual scheme and future evolution of the study area**

618 Results have showed that the Omo River planform and the surrounding area has heavily
619 changed during the last decades. Reasons for this can be found in the variation of
620 the lake level, a modified river hydrology, and a diminished sediment load. We discussed
621 above how these changes may have impacted the land coverage of the study area and river
622 morphodynamics. The main result is that the Omo River became less dynamic with time,
623 abandoning secondary/distributary channels and possibly deepening its channel bed, and
624 vegetation biomass growth in density. Studies on delta formations have shown that deltas
625 characterized by deep channels require larger disturbance to be modified (M. Van Dijk et
626 al., 2012), and their evolutionary time scales increase proportionally to the length of the
627 channel and sediment load reduction.

628 It is therefore reasonable to think that the lower reach of the Omo River and the delta
629 region have reached a new stable equilibrium state with less variations than the previous
630 one. In the past, the Omo River was highly dynamic and able to rework its morphology
631 periodically. While during floods, the deposition of fluvial bar modified the flow pattern
632 inducing channel avulsion and bifurcations. This generated new channels or widened ex-
633 isting ones that eventually were abandoned during the subsequent dry season. In order to
634 restore the previous state of the system, massive changes are required about the boundary
635 conditions imposed upstream by the dam, i.e. sediment load and water flow, downstream
636 by the lake level. This will change the channel slope and depth and reactivate that cyclic

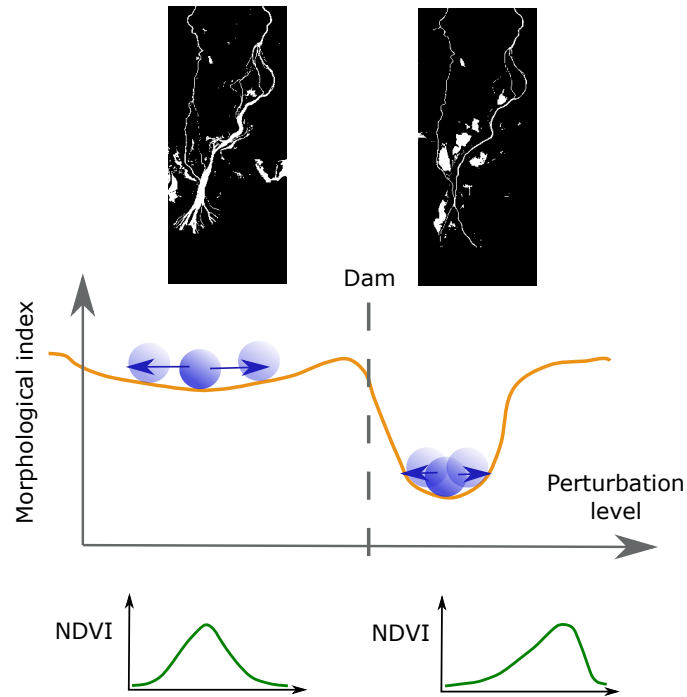


Figure 11. Conceptual model of the changes in eco-morphological processes observed for the lower reach of the Omo River.

637 process of mouth bar deposit and avulsion at the base of delta formation. Consequentially,
 638 the population of plants will change further promoting the establishment of a dynamic
 639 ecosystem.

640 Changes in climate variables should also be taken into account when considering if the
 641 river system could return to the previous, more dynamic, configuration. A recent modelling
 642 study exploring the next 20 years suggested that climate change will modify precipitation
 643 patterns increasing the magnitude and frequency of floods, and thus the overall lake inflow
 644 (UNEP-DHI-Centre, 2021). The lake level will therefore keep rising since it is unlikely that
 645 the increase in temperature observed (Figure 6a) may affect the evaporation rate such that
 646 to contrast the positive trend of the flow rate induced by more frequent rain events. On the
 647 other hand, the increasing need of water for crops irrigation within the Omo basin could
 648 affect this trend and progressively reduce the water level of the lake. The rapid expansion
 649 of cotton crops within the last years have increased the amount of water flow subtracted to
 650 the Omo River downstream the dam, reducing almost by half the base inflow of the Turkana
 651 Lake. This scenario will be further exacerbated by the application of the future cultivation
 652 plans already approved for 2025 which will further diminish the water flow of the Omo to
 653 a quarter of that initially released by the dam, and the construction of two other dams,
 654 the Gibe IV and Gibe V downstream the Gibe III. As a result, the lake level will drop
 655 with serious consequences for the fish communities particularly those close to the shores
 656 (especially during breeding season). The low water table will change the vegetation type as
 657 well as its spatial distribution, and floods will not be able to modify channel morphology.
 658 So far, studies on future trajectories have been investigating mostly lake level variations,
 659 but future research should focus also on vegetation and channel dynamics. Such studies will

660 help to identify management actions that could help to restore previous processes of the
 661 Omo river and bring the ecosystem to a new equilibrium.

662 References

- 663 Acharya, T. D., Subedi, A., & Lee, D. H. (2018). Evaluation of water indices for surface
 664 water extraction in a landsat 8 scene of nepal. *Sensors*, *18*(8), 2580.
- 665 Amri, R., Zribi, M., Lili-Chabaane, Z., Duchemin, B., Gruhier, C., & Chehbouni, A.
 666 (2011). Analysis of vegetation behavior in a north african semi-arid region, using
 667 spot-vegetation ndvi data. *Remote sensing*, *3*(12), 2568–2590.
- 668 Avery, S. (2011). Hydrological impacts of ethiopia’s omo basin on kenya’s lake turkana.
 669 *presented under “Global Programs and Strategies on Assessment and Management of*
 670 *Lakes and Their Basins: UNEP/ILEC Collaboration”, 14th World Lake Conference,*
 671 *Austin, Texas, USA, 3rd November 2011.*
- 672 Avery, S. (2012). Lake turkana & the lower omo: hydrological impacts of major dam and
 673 irrigation developments. *African Studies Centre, the University of Oxford.*
- 674 Ayalew, L. (2009). Analyzing the effects of historical and recent floods on channel pattern
 675 and the environment in the lower omo basin of ethiopia using satellite images and gis.
 676 *Environmental geology*, *58*(8), 1713–1726.
- 677 Bau’, V., Zen, S., Calvani, G., & Perona, P. (2019). Extracting the critical rooting length in
 678 plant uprooting by flow from pullout experiments. *Water Resources Research*, *55*(12),
 679 10424–10442.
- 680 Calvani, G., Perona, P., Zen, S., Solari, L., et al. (2019). Return period of vegetation
 681 uprooting by flow. *Journal of Hydrology*, *578*, 124103.
- 682 Camporeale, C., Perucca, E., Ridolfi, L., & Gurnell, A. (2013). Modeling the interactions
 683 between river morphodynamics and riparian vegetation. *Reviews of Geophysics*, *51*(3),
 684 379–414.
- 685 Caponi, F., & Siviglia, A. (2018). Numerical modeling of plant root controls on gravel bed
 686 river morphodynamics. *Geophysical Research Letters*, *45*(17), 9013–9023.
- 687 Carr, C. J. (1998). Patterns of vegetation along the omo river in southwest ethiopia. *Plant*
 688 *Ecology*, *135*(2), 135–163.
- 689 Corenblit, D., Tabacchi, E., Steiger, J., & Gurnell, A. M. (2007). Reciprocal interactions
 690 and adjustments between fluvial landforms and vegetation dynamics in river corridors:
 691 a review of complementary approaches. *Earth-Science Reviews*, *84*(1-2), 56–86.
- 692 *ECMWF.* (2021). <https://www.ecmwf.int/>. (Accessed: 2021-08-17)
- 693 Edmonds, D., & Slingerland, R. (2007). Mechanics of river mouth bar formation: Implica-
 694 tions for the morphodynamics of delta distributary networks. *Journal of Geophysical*
 695 *Research: Earth Surface*, *112*(F2).
- 696 Feyisa, G. L., Meilby, H., Fensholt, R., & Proud, S. R. (2014). Automated water extraction
 697 index: A new technique for surface water mapping using landsat imagery. *Remote*
 698 *Sensing of Environment*, *140*, 23–35.
- 699 Głogowski, A., Perona, P., Bryś, K., & Bryś, T. (2021). Nonlinear reconstruction of biocli-
 700 matic outdoor-environment dynamics for the lower silesia region (sw poland). *Inter-*
 701 *national Journal of Biometeorology*, 1–15.
- 702 Gorelick, N., Hancher, M., Dixon, M., Ilyushchenko, S., Thau, D., & Moore, R. (2017).
 703 Google earth engine: Planetary-scale geospatial analysis for everyone. *Remote Sens-*
 704 *ing of Environment*. Retrieved from <https://doi.org/10.1016/j.rse.2017.06.031>
 705 doi: 10.1016/j.rse.2017.06.031
- 706 Gurnell, A. (2014). Plants as river system engineers. *Earth Surface Processes and Land-*
 707 *forms*, *39*(1), 4–25.
- 708 Haack, B. (1996). Monitoring wetland changes with remote sensing: an east african example.
 709 *Environmental Management*, *20*(3), 411–419.
- 710 Henshaw, A. J., Gurnell, A. M., Bertoldi, W., & Drake, N. A. (2013). An assessment of
 711 the degree to which landsat tm data can support the assessment of fluvial dynamics,

- 712 as revealed by changes in vegetation extent and channel position, along a large river.
 713 *Geomorphology*, 202, 74–85.
- 714 Kim, W., & Jerolmack, D. J. (2008). The pulse of calm fan deltas. *The Journal of Geology*,
 715 116(4), 315–330.
- 716 Muñoz Sabater, J. (2019). Era5-land monthly averaged data from 1981 to present. *Coperni-*
 717 *cus Climate Change Service (C3S) Climate Data Store (CDS)*. (Accessed: 2021-08-17),
 718 doi:10.24381/cds.68d2bb30.
- 719 Nepf, H. M. (2012). Hydrodynamics of vegetated channels. *Journal of Hydraulic Research*,
 720 50(3), 262–279.
- 721 Nittrouer, J. A., Shaw, J., Lamb, M. P., & Mohrig, D. (2012). Spatial and temporal trends
 722 for water-flow velocity and bed-material sediment transport in the lower mississippi
 723 river. *Bulletin*, 124(3-4), 400–414.
- 724 Piliouras, A., & Kim, W. (2019). Delta size and plant patchiness as controls on channel
 725 network organization in experimental deltas. *Earth Surface Processes and Landforms*,
 726 44(1), 259–272.
- 727 Politti, E., Bertoldi, W., Gurnell, A., & Henshaw, A. (2018). Feedbacks between the
 728 riparian salicaceae and hydrogeomorphic processes: A quantitative review. *Earth-*
 729 *Science Reviews*, 176, 147–165.
- 730 Reitz, M. D., Jerolmack, D. J., & Swenson, J. B. (2010). Flooding and flow path selection
 731 on alluvial fans and deltas. *Geophysical Research Letters*, 37(6).
- 732 Rouse, J. W., Haas, R. H., Schell, J. A., Deering, D. W., & Harlan, J. C. (1974). Monitoring
 733 the vernal advancement and retrogradation (green wave effect) of natural vegetation.
 734 *NASA/GSFC Type III Final Report, Greenbelt, Md*, 371.
- 735 Tian, F., Brandt, M., Liu, Y. Y., Verger, A., Tagesson, T., Diouf, A. A., ... Fensholt, R.
 736 (2016). Remote sensing of vegetation dynamics in drylands: Evaluating vegetation
 737 optical depth (vod) using avhrr ndvi and in situ green biomass data over west african
 738 sahel. *Remote Sensing of Environment*, 177, 265–276.
- 739 Tron, S., Perona, P., Gorla, L., Schwarz, M., Laio, F., & Ridolfi, L. (2015). The signature of
 740 randomness in riparian plant root distributions. *Geophysical Research Letters*, 42(17),
 741 7098–7106.
- 742 UNEP-DHI-Centre. (2021). Support to sustainable development in lake turkana and its river
 743 basins. results of modelling of future scenarios of lake turkana and its river basins.
 744 (United Nations Environment Programme (UNEP), Technical Report)
- 745 *USGS-Landsat7*. (2021). [https://www.usgs.gov/core-science-systems/nli/landsat/
 746 landsat-7?qt-science_support_page_related_con=0#qt-science_support_page
 747 _related_con](https://www.usgs.gov/core-science-systems/nli/landsat/landsat-7?qt-science_support_page_related_con=0#qt-science_support_page_related_con). (Accessed: 2021-08-18)
- 748 Van Dijk, M., Kleinhans, M. G., Postma, G., & Kraal, E. (2012). Contrasting morphody-
 749 namics in alluvial fans and fan deltas: effect of the downstream boundary. *Sedimen-*
 750 *tology*, 59(7), 2125–2145.
- 751 Van Dijk, W., Teske, R., Van de Lageweg, W., & Kleinhans, M. (2013). Effects of vegeta-
 752 tion distribution on experimental river channel dynamics. *Water Resources Research*,
 753 49(11), 7558–7574.
- 754 Wang, J., Muto, T., Urata, K., Sato, T., & Naruse, H. (2019). Morphodynamics of river
 755 deltas in response to different basin water depths: An experimental examination of
 756 the grade index model. *Geophysical Research Letters*, 46(10), 5265–5273.
- 757 Zaniolo, M., Giuliani, M., Sinclair, S., Burlando, P., & Castelletti, A. (2021). When
 758 timing matters—misdesigned dam filling impacts hydropower sustainability. *Nature*
 759 *Communications*, 12.
- 760 Zen, S., & Perona, P. (2020). Biomorphodynamics of river banks in vegetated channels with
 761 self-formed width. *Advances in Water Resources*, 135, 103488.
- 762 Zen, S., Zolezzi, G., Toffolon, M., & Gurnell, A. M. (2016). Biomorphodynamic modelling
 763 of inner bank advance in migrating meander bends. *Advances in Water Resources*,
 764 93, 166–181.